

Coronal Magnetometry with EUV Permitted LinesNATALIIA G. SHCHUKINA,^{1,2,3} JAVIER TRUJILLO BUENO,^{1,2,4} SUPRIYA HEBBUR DAYANANDA,^{1,2} RAFAEL MANSO SAINZ,⁵ AND ANDRII V. SUKHORUKOV^{1,2,3}¹*Instituto de Astrofísica de Canarias, E-38205 La Laguna, Tenerife, Spain*²*Dpto. de Astrofísica, Universidad de La Laguna, E-38206 La Laguna, Tenerife, Spain*³*Main Astronomical Observatory, National Academy of Sciences, 03143 Kyiv, Ukraine*⁴*Consejo Superior de Investigaciones Científicas, Spain*⁵*Third Institute of Physics, University of Göttingen, Friedrich-Hund-Platz 1, 37077 Göttingen, Germany*

(Accepted for publication in The Astrophysical Journal)

ABSTRACT

A major challenge in solar physics is to obtain empirical information on the magnetic field of the million-degree plasma of the solar corona. To this end, we need observables of the solar radiation sensitive to the coronal magnetic field. The most familiar observables are the polarization signals of visible and near-infrared forbidden lines of highly ionized species and some ultraviolet permitted lines, like hydrogen Lyman- α . While the coronal radiation in these spectral lines can only be detected for off-limb line of sights, the coronal radiation from permitted extreme ultraviolet (EUV) lines can be observed also on the solar disk. These coronal lines are mainly collisionally excited, but it has been pointed out that some permitted EUV lines can actually be linearly polarized if their lower level carries atomic alignment, and that their linear polarization is sensitive to the orientation of the coronal magnetic field (see [Manso Sainz & Trujillo Bueno 2009](#)). Here we theoretically investigate the linear polarization in permitted EUV lines of a variety of ions: Fe X, Fe XI, Fe XIII, Fe XIV, Si IX, and Si X. To this end, we have developed a numerical code, which we have applied to investigate the linear polarization and magnetic sensitivity of many permitted EUV lines in a one-dimensional model of the solar corona, providing a list of the most promising lines to be further investigated for polarimetry with future space telescopes. Our next step will be to extend this work by using state-of-the-art three-dimensional coronal models.

Keywords: line: profiles — polarization — radiative transfer — Sun: corona**1. INTRODUCTION**

If collisions of the coronal ions with electrons and protons are assumed to be isotropic, then the ensuing collisional transitions cannot induce *directly* atomic level polarization (i.e., population imbalances and quantum coherence between the magnetic sublevels pertaining to the J -levels of the coronal ions, J being the total angular momentum of the atomic level under consideration). Under the common assumption of isotropic inelastic collisions the only mechanism capable of directly inducing atomic level polarization is through radiative transitions driven by an anisotropic radiation field. At coronal heights the underlying solar disk is practically dark

at the extreme ultraviolet (EUV) wavelengths of the permitted line transitions investigated here, which have wavelengths $\lambda < 250$ Å. However, the solar disk is very bright at the visible and near-infrared (IR) wavelengths of the forbidden transitions that take place between the J -levels of the ground-term of the coronal ions. The ensuing anisotropic radiation pumping at the forbidden-line wavelengths produces atomic polarization in the J -levels of the ground terms of the coronal ions. This radiatively-induced atomic level polarization can be partly transferred to the upper levels of the EUV permitted transitions via the isotropic collisions with electrons and protons that excite such upper levels. As a result, the spontaneously emitted EUV line radiation can be linearly polarized. A detailed explanation of this polarization mechanism of EUV coronal lines, with analytical and numerical results, can be found in [Manso Sainz & Trujillo Bueno \(2009\)](#).

In Manso Sainz & Trujillo Bueno (2009) it is shown quantitatively that the radiation emitted in the permitted Fe X lines at 174.5 Å and 177 Å turns out to be linearly polarized, both for off-limb and on-disk lines of sight. First, scattering of continuum radiation in the forbidden (magnetic dipole) 6376.29 Å line generates atomic polarization in the $J = \frac{3}{2}$ level of the ground term $^2P^o$. Then, collisional transitions pump this radiatively-induced ground-level atomic polarization to the excited levels of the coronal ions. As a result, the spontaneous emission from the upper level of the permitted EUV line under consideration can be partially polarized. The resulting linear polarization is sensitive to the electron density and to the orientation of the magnetic field in the observed coronal plasma structure. The aim of this paper is to investigate in detail the linear polarization that this mechanism introduces in the EUV permitted lines of many highly ionized atoms of the solar corona, and to evaluate their diagnostic potential for coronal magnetic field measurements. In addition to Fe X, we consider the following coronal ions: Fe XI, Fe XIII, Fe XIV, Si IX, and Si X.

In this first paper our strategy is the following. We consider a spherically symmetric one-dimensional (1D) model of the quiet solar corona (Del Zanna & DeLuca 2018), which gives the temperature and the electron density as a function of height above the solar limb. For each height in the model atmosphere we solve the statistical equilibrium equations for the elements of the atomic density matrix (Landi Degl’Innocenti & Landolfi 2004), taking into account the continuum radiation reaching each height from the quiet Sun disk. This allows us to compute the emissivities in the various Stokes parameters and to compute the emergent wavelength-integrated Stokes signals as a function of height. In this first paper we consider the limit of single scattering events in the plane of the sky (POS), while in a next paper we will investigate the impact of the integration along the line of sight (LOS).

Some authors have studied the possible impact of resonance scattering on some EUV coronal lines (e.g., Withbroe & Raymond 1984; Raouafi et al. 1999, 2002; Supriya et al. 2021; Khan et al. 2024; Seaton et al. 2025). The wavelengths of the EUV coronal lines investigated in this paper are mainly below 250 Å, and we have assumed that the excitation of their upper levels is dominated by inelastic collisions with electrons (i.e., that at the coronal heights where the EUV line radiation is emitted by the million-degree plasma there is no significant radiative excitation of the ions). Therefore, the linear polarization signals of the EUV permitted lines investigated in this paper are only due to the mechanism explained in Manso Sainz & Trujillo Bueno (2009). We leave for a future investigation the possibility of anisotropic radiation pumping at the short EUV line wavelengths considered here. For a recent review on mag-

netic field diagnostics in the solar upper atmosphere see Trujillo Bueno & del Pino Alemán (2022).

The structure of the paper is as follows. In Section 2 we formulate the problem and explain the methods of solution we have implemented. The atmospheric model and the atomic data used in the calculations are described in Section 3, and the results are presented in Section 4. Our selection of the most promising EUV lines is presented in Section 5. Section 6 summarizes our main conclusions and discusses the next steps of our investigation.

2. FORMULATION OF THE PROBLEM

We formulate the problem within the framework of the density matrix theory of polarization in spectral lines described in Landi Degl’Innocenti & Landolfi (2004), which is valid if the incident radiation field is flat across a frequency range wider than both the Larmor frequency of the ambient magnetic field and the inverse lifetime of the levels. As a matter of fact, at the wavelengths of the forbidden line transitions the (visible and near-IR) solar-disk continuum radiation that illuminates the coronal ions is nearly spectrally flat, while at the EUV wavelengths of the permitted line transitions the underlying solar disk is practically dark.

The radiation field is quantified by the radiation field tensors J_Q^K , with $K = 0, 1, 2$ and $-K \leq Q \leq K$ (see equation 5.157 in the quoted monograph). We assume that the radiation that illuminates the coronal ions at any given height above the Sun’s visible limb is the continuum radiation coming from the underlying solar disk, and that it is unpolarized and axially symmetric around the solar radius vector through the considered spatial point in the corona (hereafter, the local vertical direction). Therefore, in the reference system where the Z-axis is along the local vertical direction (hereafter, the ‘vert’ reference system) the only non-zero components of the radiation field tensors are the mean intensity

$$[J_0^0]_{\text{vert}} = \frac{1}{2} \int d\mu I(\nu, \mu), \quad (1)$$

and the radiation anisotropy

$$[J_0^2]_{\text{vert}} = \frac{1}{4\sqrt{2}} \int d\mu (3\mu^2 - 1) I(\nu, \mu), \quad (2)$$

where $\mu = \cos\theta$ (with θ the angle between the ray path and the vertical), ν is the frequency of the incident radiation beam, and $I(\nu, \mu)$ the intensity.

We calculate the $[J_0^0]_{\text{vert}}$ and $[J_0^2]_{\text{vert}}$ components following section 12.3 of Landi Degl’Innocenti & Landolfi (2004), which uses a quadratic expansion of the limb darkening law ($N = 2$ in their equation 12.31). To this end, we have used the center-to-limb variation of the *observed* solar continuum intensity $I(\lambda, \theta)/I(\lambda, 0)$ given by Allen (1976) in page 171. The absolute continuum intensity at the solar disk

center $I(\lambda, 0)$ measured between the spectral lines is taken also from Allen (1976, see the Table in page 172).

In the reference system where the Z-axis is along the direction of the ambient magnetic field (hereafter, the ‘mag.field’ reference system) the ensuing radiation field tensors, $[J_Q^K]_{\text{mag.field}}$, can be obtained from the $[J_Q^K]_{\text{vert}}$ ones by rotation, as indicated by equation (13.14) of Landi Degl’Innocenti & Landolfi (2004). Given that the incident radiation field is assumed to be unpolarized and the only non-zero $[J_Q^K]_{\text{vert}}$ components are $[J_0^0]_{\text{vert}}$ and $[J_0^2]_{\text{vert}}$, the components $[J_Q^1]_{\text{mag.field}} = 0$. Moreover, it is useful to note that

$$[J_0^0]_{\text{mag.field}} = [J_0^0]_{\text{vert}}, \quad (3)$$

and

$$[J_0^2]_{\text{mag.field}} = \frac{1}{2} (3\cos^2\theta_B - 1) [J_0^2]_{\text{vert}}, \quad (4)$$

where θ_B is the angle between the magnetic field vector and the local vertical.

For the coronal ions investigated here (Fe X, Fe XI, Fe XIII, Fe XIV, Si IX, and Si X) we can consider atomic models without hyperfine structure described in the Russell-Saunders coupling scheme. Therefore, the energy levels are characterized by the quantum numbers α (a set of quantum numbers describing the electronic configuration, the total orbital angular momentum, and the total electronic spin) and J (the level’s total angular momentum). The state of each (αJ) atomic level is quantified by the multipolar components $\rho_Q^K(\alpha J)$ of the atomic density matrix, with $K = 0, 1, \dots, 2J$ and $-K \leq Q \leq K$ (see Table 3.6 in Landi Degl’Innocenti & Landolfi 2004). In particular, $\rho_0^0(\alpha J)$ is proportional to the level’s overall population, $\rho_0^2(\alpha J)$ is the alignment coefficient that quantifies the degree of population imbalance between magnetic sublevels having different absolute value of the magnetic quantum numbers M , while $\rho_Q^2(\alpha J)$ with $Q \neq 0$ are linear combinations of the quantum coherences between magnetic sublevels whose quantum number M differ by Q (hereafter, coherences). In order to find the $\rho_Q^K(\alpha J)$ components corresponding to each (αJ) -level we have to solve the statistical equilibrium equations (see chapter 7 in Landi Degl’Innocenti & Landolfi 2004), which account for collisional transitions (dependent on the local electron density and temperature in the coronal plasma) and radiative transitions (the calculation of which requires taking into account the anisotropy of the continuum radiation coming from the underlying solar disk). For the coronal ions the separation in frequency units between the J -levels is much larger than their natural width. This and the assumption that the solar corona is optically thin at the wavelengths of the considered line transitions imply that we can safely ignore any significant impact due to quantum mechanical interference between the magnetic sub-

levels pertaining to different J -levels. Therefore, the relevant statistical equilibrium equations are those corresponding to the multilevel atom model described in chapter 7 of Landi Degl’Innocenti & Landolfi (2004).

The permitted EUV coronal lines considered in this paper are electric dipole (E1) transitions between short-lived upper levels u and long-lived lower levels ℓ . As summarized above, the atomic polarization of the lower level of the line transitions is caused by anisotropic continuum radiation pumping in the magnetic dipole (M1) forbidden line transitions, which lie at visible and near infrared (IR) wavelengths, while the atomic polarization in the upper level of the EUV lines results from the transfer to the upper levels of such lower-level polarization via isotropic collisions (Manso Sainz & Trujillo Bueno 2009).

The Hanle effect is the magnetic-field-induced modification of the atomic level polarization (e.g., Trujillo Bueno 2001), and the critical magnetic field strength for producing a sizable impact on the polarization of the atomic level of angular momentum J under consideration is¹

$$B_H = \frac{1.137 \times 10^{-7}}{t_{\text{life}} g_J}, \quad (5)$$

where t_{life} is the level’s radiative lifetime, in seconds, and g_J the Landé factor of the J -level under consideration. Approximately, the sensitivity of a spectral line to the Hanle effect occurs for magnetic strengths (B) between $0.2B_H$ and $5B_H$. For $B \gg 5B_H$ the line is in the saturation regime of the Hanle effect, in which there are no quantum coherences in the magnetic field reference frame and the line’s linear polarization is sensitive only to the magnetic field orientation (see Landi Degl’Innocenti & Landolfi 2004).

The following two points are very important for understanding the formulation of the problem.

First, the lower levels of the EUV line transitions investigated here have very long lifetimes, because they belong to the ground term of the considered ion. As a result, the critical magnetic field strength for the Hanle effect in the lower level of the considered EUV lines is $B_H < 10^{-5}$ G. Given that the magnetic fields of the 10^6 K plasma of the solar corona are much larger, the lower levels of our EUV line transitions are in the saturation regime of the Hanle effect (e.g., Landi Degl’Innocenti & Landolfi 2004). For this reason, and recalling that the incident radiation field is assumed to be unpolarized, in the reference frame in which the quantization axis of total angular momentum is parallel to the magnetic field vector (i.e., the magnetic field reference frame) there is no quantum coherence between the magnetic sublevels of such lower levels (i.e., in the magnetic field reference frame

¹ This basic formula results from equating the Zeeman splitting of the level with its natural width.

the only non-vanishing multipolar components of the lower-level atomic density matrix are $\rho_0^K(\alpha J_l)$, and with K even because $[J_Q^1]_{\text{vert.}} = [J_Q^1]_{\text{mag.field}} = 0$.

Second, since we are assuming that only isotropic collisions with electrons and protons can excite the upper levels of the EUV permitted lines considered here, it is clear that in the magnetic field reference frame the only possible multipolar components of the upper-level atomic density matrix are $\rho_0^K(\alpha_u J_u)$ because, as explained above, in the lower levels of the EUV lines there are no coherences in the magnetic field reference frame. Without upper-level coherences in the magnetic field reference frame there is no Hanle effect in the EUV lines (see section 10.3 of Landi Degl'Innocenti & Landolfi 2004). Nevertheless, the Einstein coefficient $A(\alpha_u J_u \rightarrow \alpha_l J_l)$ for spontaneous emission from the upper to the lower level in the EUV lines investigated here is of the order of 10^{10} s^{-1} , or larger, and the lifetime of the line's upper level is $t_{\text{life}} = 1/\sum_{i < u} A(\alpha_u J_u \rightarrow \alpha_i J_i)$. For this reason, and noting that $g_J \sim 1$, the critical magnetic field for the Hanle effect in the upper level of our EUV lines that results from the application of Equation (5) is $B_H > 2000 \text{ G}$. Therefore, even if the above-mentioned coherences were present in the upper levels of our EUV lines (e.g., because of a significant anisotropic radiation pumping at the EUV line wavelengths) there would be no Hanle effect because the magnetic fields of the 10^6 K coronal plasma are much weaker than 2000 G .

Because of the two reasons mentioned above, in the magnetic field reference frame the only multipolar components of the atomic density matrix that quantify the state of any J level are $[\rho_0^K(\alpha J)]_{\text{mag.field}}$. These multipolar components can be found by solving the statistical equilibrium equations of the so-called no-coherence case (see section 7.4 of Landi Degl'Innocenti & Landolfi 2004).

Since the critical magnetic field for the upper-level Hanle effect is much larger than the coronal magnetic field strength, and the lower level is in its Hanle saturation regime, it is important to note that the linear polarization in the EUV lines investigated in this paper is sensitive only to the orientation of the coronal magnetic field, but not to its strength. Clearly, the linear polarization amplitudes are also sensitive to the plasma electron density and temperature.

We do not consider the Stokes V signals because they are negligible for the EUV lines of the solar corona. This is because for coronal temperatures in the range $10^5 - 10^6 \text{ K}$ the typical Doppler width of the EUV lines of iron ions is at least two or three orders of magnitude larger than the Zeeman splitting due to the coronal magnetic fields.

2.1. Emission coefficients

The expressions of the emission coefficients in the I , Q , and U Stokes parameters of the permitted EUV-line radiation emitted along the direction $\vec{\Omega}_o$ take a particularly simple

form when choosing the positive Stokes- Q reference direction along the *perpendicular* to the projection of the magnetic field vector onto the plane perpendicular to $\vec{\Omega}_o$ (see Landi Degl'Innocenti & Landolfi 2004):

$$\varepsilon_I(\nu, \vec{\Omega}_o) = C \left[1 + \frac{1}{2\sqrt{2}} (3\cos^2\Theta - 1) w_{J_u J_\ell}^{(2)} \sigma_0^2(\alpha_u J_u) \right] \phi(\nu), \quad (6)$$

$$\varepsilon_Q(\nu, \vec{\Omega}_o) = C \frac{3}{2\sqrt{2}} \sin^2\Theta w_{J_u J_\ell}^{(2)} \sigma_0^2(\alpha_u J_u) \phi(\nu), \quad (7)$$

$$\varepsilon_U(\nu, \vec{\Omega}_o) = 0, \quad (8)$$

where

$$C = \frac{h\nu}{4\pi} N(\alpha_u J_u) A(\alpha_u J_u \rightarrow \alpha_\ell J_\ell),$$

Θ is the angle between the magnetic field vector and the direction $\vec{\Omega}_o$, h the Planck constant, ν the frequency of the transition, $A(\alpha_u J_u \rightarrow \alpha_\ell J_\ell)$ the Einstein coefficient for spontaneous emission from the upper to the lower level, $\phi(\nu)$ the normalized line profile, and J_u and J_ℓ the total angular momenta for the upper and lower levels. The population of the upper level is

$$N(\alpha_u J_u) = N(\text{ion}) \sqrt{(2J_u + 1)} \rho_0^0(\alpha_u J_u), \quad (9)$$

with $N(\text{ion})$ being the total number of the ions of given type per unit volume.

The fractional alignment $\sigma_0^2(\alpha_u J_u)$ of the upper level entering in Equations (6) and (7) is

$$\sigma_0^2(\alpha_u J_u) = \rho_0^2(\alpha_u J_u) / \rho_0^0(\alpha_u J_u), \quad (10)$$

where the density matrix element $\rho_0^2(\alpha_u J_u)$ is that defined in the magnetic reference frame.

2.2. The statistical equilibrium equations

Given that we are assuming that at EUV wavelengths there is no anisotropic radiation pumping and that isotropic collisions with electrons and protons dominate the excitation of the upper levels of the permitted lines in our multilevel atomic models, there are no coherences in the magnetic field reference frame. Therefore, the non-vanishing multipolar components $\rho_0^K(\alpha J)$ of the atomic density matrix in the magnetic field reference frame can be found by solving the statistical equilibrium equations of the no-coherence case explained in section 7.4 of Landi Degl'Innocenti & Landolfi (2004). Such equations are the following:

$$\begin{aligned}
\frac{d}{dt}\rho_0^K(\alpha J) = & \sum_{\alpha_\ell J_\ell K_\ell} \rho_0^{K_\ell}(\alpha_\ell J_\ell) t_A(\alpha JK, \alpha_\ell J_\ell K_\ell) \\
& + \sum_{\alpha_u J_u K_u} \rho_0^{K_u}(\alpha_u J_u) t_E(\alpha JK, \alpha_u J_u K_u) \\
& + t_S(\alpha JK, \alpha_u J_u K_u) \Big] \\
& - \sum_{K'} \rho_0^{K'} [r_A(\alpha JK K') + r_E(\alpha JK K') + r_S(\alpha JK K')] \\
& + \sum_{\alpha_\ell J_\ell} \sqrt{\frac{2J_\ell + 1}{2J + 1}} C_I^{(K)}(\alpha J, \alpha_\ell J_\ell) \rho_0^K(\alpha_\ell J_\ell) \\
& + \sum_{\alpha_u J_u} \sqrt{\frac{2J_u + 1}{2J + 1}} C_S^{(K)}(\alpha J, \alpha_u J_u) \rho_0^K(\alpha_u J_u) \\
& - \left[\sum_{\alpha_u J_u} C_I^{(0)}(\alpha_u J_u, \alpha J) + \sum_{\alpha_\ell J_\ell} C_S^{(0)}(\alpha_\ell J_\ell, \alpha J) \right. \\
& \left. + D^{(K)}(\alpha J) \right] \rho_0^K(\alpha J) = 0. \quad (11)
\end{aligned}$$

For dipole transitions ($\Delta J = 0, \pm 1, 0 \nrightarrow 0$), the expressions for the transfer rates due to absorptions (t_A), stimulated emissions (t_S), and spontaneous emissions (t_E), as well as the expressions for the relaxation rates due to absorptions (r_A), stimulated emissions (r_S), and spontaneous emissions (r_E), can be found in equations (7.20) of [Landi Degl'Innocenti & Landolfi \(2004\)](#). With the exception of t_E and r_E , all the other transfer and relaxation rates contain the radiation field tensors $[J_0^0]_{\text{mag.field}}$ and $[J_0^2]_{\text{mag.field}}$ given by Eqs. (3) and (4), which are the only relevant ones in the research problem under consideration. In Eq. (11) the quantities $C_I^{(K)}$ and $C_S^{(K)}$ are the multipole components of the inelastic and superelastic collisional rates, respectively, and $D^{(K)}$ are the depolarizing rates due to elastic collisions (see equations 7.87, 7.89, 7.102, and 7.100 of [Landi Degl'Innocenti & Landolfi \(2004\)](#)).

As indicated in Equation (11) we assume statistical equilibrium (i.e., $\frac{d}{dt}\rho_0^K(\alpha J) = 0$). The determinant of this system of statistical equilibrium equations is zero and is the reason why its solution would give the $\rho_0^K(\alpha J)$ components up to a multiplicative factor. To obtain the solution for the $\rho_0^K(\alpha J)$ components, we add the trace equation

$$\sum_{\alpha J} \frac{N(\alpha J)}{N(\text{ion})} = \sum_{\alpha J} \sqrt{2J + 1} \rho_0^0(\alpha J) = 1 \quad (12)$$

The level populations $N(\alpha J)$ needed for calculating the emission coefficients $\varepsilon_I(\nu, \Theta)$ and $\varepsilon_Q(\nu, \Theta)$ were obtained using

$$N(\alpha J) = \frac{N(\alpha J)}{N(\text{ion})} \frac{N(\text{ion})}{N(\text{el})} \frac{N(\text{el})}{N_H} \frac{N_H}{N_e} N_e, \quad (13)$$

where $N(\text{el})/N_H$ is the abundance of the element under consideration relative to hydrogen and N_H/N_e is the hydro-

gen abundance relative to the electron density. The relative level population $N(\alpha J)/N(\text{ion})$ is obtained from the solution of Equations (11) and (12). The ionization fraction $N(\text{ion})/N(\text{el})$ was taken from CHIANTI Version 10 database ([Del Zanna et al. 2021](#)). The ratio N_H/N_e is in the range $\sim 0.8 - 0.9$, since for coronal temperatures hydrogen and helium are fully ionized ([Del Zanna & Mason 2018](#)). In our study we adopt a proton-to-electron density ratio of 0.85.

As explained in [Landi Degl'Innocenti & Landolfi \(2004\)](#), the interaction between the ions and the colliders (e.g., electrons) is described by a sum of tensor operators of rank K acting on the state vectors of the ion. Fortunately, in many cases, the interaction is suitably described by just one operator of rank \tilde{K} , so that the multipole components $C_I^{(K)}$ and $C_S^{(K)}$ are related to the corresponding multipole components of rank 0 by the following equations (see Appendix 4 of [Landi Degl'Innocenti & Landolfi \(2004\)](#)):

$$C_I^{(K)}(\alpha J, \alpha_\ell J_\ell) = (-1)^K \frac{\left\{ \begin{matrix} J & J & K \\ J_\ell & J_\ell & \tilde{K} \end{matrix} \right\}}{\left\{ \begin{matrix} J & J & 0 \\ J_\ell & J_\ell & \tilde{K} \end{matrix} \right\}} C_I^{(0)}(\alpha J, \alpha_\ell J_\ell) \quad (14)$$

$$C_S^{(K)}(\alpha J, \alpha_u J_u) = (-1)^K \frac{\left\{ \begin{matrix} J & J & K \\ J_u & J_u & \tilde{K} \end{matrix} \right\}}{\left\{ \begin{matrix} J & J & 0 \\ J_u & J_u & \tilde{K} \end{matrix} \right\}} C_S^{(0)}(\alpha J, \alpha_u J_u), \quad (15)$$

where the curly bracket terms are the Wigner 6- j symbols. We have $\tilde{K} = 1$ for the E1 transitions and $\tilde{K} = 2$ for the E2 transitions.

Note that in the notation used by [Mihalas \(1978\)](#) the components of the inelastic $C_I^{(0)}$ and superelastic $C_S^{(0)}$ electron collisional rates are

$$C_I^{(0)}(\alpha_u J_u, \alpha_\ell J_\ell) = C_{\ell u} \quad (16)$$

and

$$C_S^{(0)}(\alpha_\ell J_\ell, \alpha_u J_u) = C_{u\ell}, \quad (17)$$

where $C_{\ell u}$ denotes the inelastic electron collisional rate for the transition from the lower level ℓ to the upper level u , while $C_{u\ell}$ denotes the superelastic electron collisional rate for the transition from the level u to the level ℓ .

As in most spectroscopic diagnostics of the solar corona, we assume that the electron and ion velocities follow a Maxwell-Boltzmann distribution with an electron temperature T_e ([Del Zanna & DeLuca 2018](#)). In this case

$$C_{\ell u} = 8.63 \cdot 10^{-6} N_e \frac{\Upsilon_{\ell u}(T_e)}{g_\ell \sqrt{T_e}} \exp(-\Delta E_{\ell u}/k_B T_e), \quad (18)$$

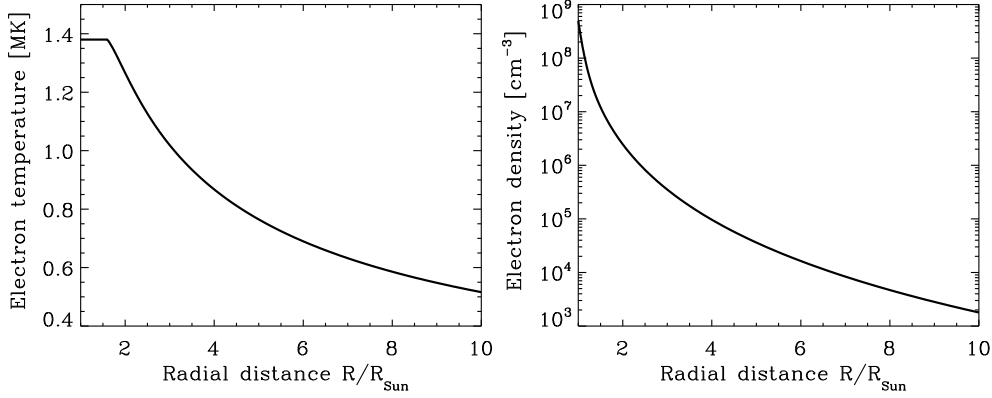


Figure 1. Electron temperature (left panel) and electron density (right panel) as a function of the radial distance R/R_{Sun} , where R_{Sun} is the solar radius in spherically symmetric 1D coronal model of the quiet Sun (Del Zanna & DeLuca 2018).

where N_e is the electron density in cm^{-3} , T_e in K, k_B is the Boltzmann constant, $g_\ell = 2J_\ell + 1$ is the statistical weight of the lower level, $\Delta E_{\ell u}$ is the transition energy, and the thermally averaged collision strength is

$$\Upsilon_{\ell u} = \int_0^\infty \Omega_{\ell u} \exp\left(-\frac{E_u}{k_B T_e}\right) d\left(\frac{E_u}{k_B T_e}\right) \quad (19)$$

with E_u the colliding electron energy after excitation and $\Omega_{\ell u}$ the collision strength between levels ℓ and u depending on $E_u/\Delta E_{\ell u}$.

For transitions other than E1 and E2 we calculated the multipolar components of the electron collisional rates adopting the strong coupling approximation (e.g., Judge et al. 2006; Schad & Dima 2020).

The depolarizing rates $D^{(K)}$ due to elastic collisions with neutral hydrogen atoms included in Equation (11) were estimated using Equation (7.108) of Landi Degl’Innocenti & Landolfi (2004). As expected, it turns out that in the quiet solar corona where the neutral hydrogen number density is small (less than 100 cm^{-3}) the sum of the inelastic and superelastic collisional rate components $\left[\sum_{\alpha_u J_u} C_I^{(0)}(\alpha_u J_u, \alpha J) + \sum_{\alpha_\ell J_\ell} C_S^{(0)}(\alpha_\ell J_\ell, \alpha J)\right]$ for each level αJ in Equation (11) is on average more than eight orders of magnitude larger than the depolarizing elastic rate $D^{(K)}(\alpha J)$. Therefore, in all our calculations we neglected such elastic collisions.

Moreover, we did not include inelastic and superelastic collisions with protons, because our estimations show that, for transitions to the highly excited levels of the ions under consideration, the proton collisional rates are much smaller (see, Bhatia & Doschek 1995, for example) than the electron collisional rates given in CHIANTI database (Del Zanna et al. 2015, 2021; Dufresne et al. 2024). We also neglected the proton collisions for transition between the J -levels of the ground terms, because they become important only for electron temperatures $T_e > 3 \times 10^6 \text{ K}$.

3. THE CORONAL MODEL AND THE ATOMIC DATA

3.1. Coronal model

We use the spherically symmetric 1D model of the quiet-Sun corona proposed by Del Zanna & DeLuca (2018). As seen in the left panel of Figure 1, the model’s electron temperature is constant ($T_e \approx 1.38 \times 10^6 \text{ K}$) for radial distances $R/R_{\text{Sun}} \leq 1.5$ while in higher layers the temperature follows the average of the polar and equator models given in Vázquez et al. (2003), decreasing till about half a million Kelvin at $R/R_{\text{Sun}} = 10$. The right panel of this Figure gives the model’s electron number density, as taken by Del Zanna & DeLuca (2018) from Gibson et al. (1999), which goes from 10^9 cm^{-3} at the model’s surface to about 10^3 cm^{-3} at $R/R_{\text{Sun}} = 10$. At each height in the coronal model we use the corresponding electron temperature and electron density to calculate the level populations $N(\alpha J)$ from Equations (9) and (13), and then apply Equations (6) and (7) to determine the Stokes emissivity coefficients ε_I and ε_Q .

3.2. Chemical abundances

For the abundance of iron and silicon we used $A_{\text{Fe}} = 7.50$ and $A_{\text{Si}} = 7.51$, respectively, which are the photospheric values recommended by Asplund et al. (2009). The A_{Fe} value agrees with the one obtained by Shchukina & Trujillo Bueno (2001) without assuming local thermodynamic equilibrium (LTE), and it is only 0.04 dex larger than the value later reported by Asplund et al. (2021). The A_{Si} value is 0.04 dex lower than the non-LTE abundance value determined by Shchukina et al. (2012), but it coincides with the value recommended by Asplund et al. (2021).

Photospheric abundances are often used in investigations of the solar corona. For example, they are used in the CHIANTI database (Del Zanna et al. 2015; Del Zanna & Mason 2018), in studies of quiet and active regions in the solar corona (see Testa et al. 2023, and references therein), as well

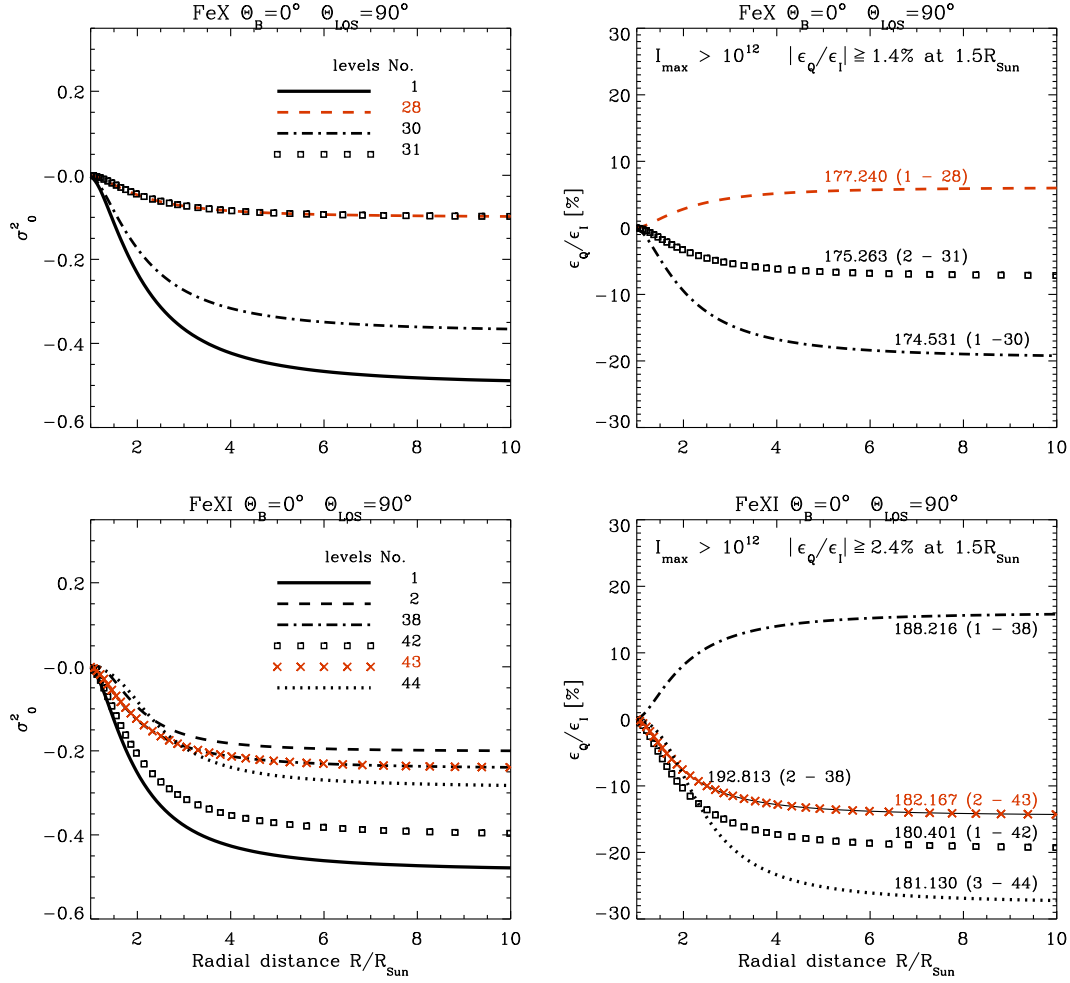


Figure 2. The fractional alignment $\sigma_0^2(\alpha J)$ of the lower and highly excited levels (left panels) and the ratio of the Stokes Q and I emission coefficients $\epsilon_Q(\nu, \Theta)/\epsilon_I(\nu, \Theta)$ (right panels) for selected EUV lines of the Fe X and Fe XI ions as a function of the radial distance R/R_{Sun} in the spherically symmetric coronal model of the quiet Sun of Del Zanna & DeLuca (2018). The top and bottom panels show the results for the Fe X and Fe XI ions, respectively. The level numbers, wavelengths, and transitions (in brackets) are indicated in the respective panels. Geometrical configuration (Θ_{LOS} is the angle between the solar radius vector through the observed point and the LOS): off-limb observations ($\Theta_{\text{LOS}} = 90^\circ$) of a radial magnetic field ($\Theta_B = 0^\circ$). For all the Fe X and Fe XI lines shown, the intensity I_{max} at $R/R_{\text{Sun}} = 1.0$ (in units of 10^{11} photons $\text{cm}^{-2} \text{s}^{-1} \text{sr}^{-1}$) and the absolute ratio $|\epsilon_Q/\epsilon_I|$ at a radial distance of $R/R_{\text{Sun}} = 1.5$ are equal to or greater than the values specified at the top of the right panels. The positive Stokes- Q direction is the perpendicular to the magnetic field.

as in simulations of polarized emission in forbidden coronal lines (e.g., Casini & Judge 1999; Schad & Dima 2020, 2021; Supriya et al. 2025).

We are aware that the chemical composition of the corona is still under debate. In particular, the coronal abundances of low First Ionization Potential (FIP) elements, such as Mg, Si, Fe, used in the latest CHIANTI version 11 database (Dufresne et al. 2024) are typically higher by a factor of 2 to 4 compared to their photospheric values. Moreover, the abundances of these chemical elements seem to vary substantially in solar regions with different magnetic topologies, such as post-flare loops, active region outflows and coronal mass ejections (see Schmelz et al. 2012; Laming 2015;

Del Zanna & Mason 2018; Testa et al. 2023; Dufresne et al. 2024, and references therein).

Therefore, neglecting the FIP effect (i.e. using the smaller photospheric Fe and Si abundances) may result in an underestimation of the Stokes I and Q emission coefficients. However, this does not affect the fractional atomic alignment σ_0^2 and the fractional linear polarizations Q/I and U/I of the EUV lines under consideration.

3.3. Atomic data

The atomic data for the Fe X, Fe XI, Fe XIII, Fe XIV, Si IX, and Si X ions, including the line identifications, level energies, collision strengths, and the Einstein coefficients for spontaneous emission, are discussed in detail in several papers (e.g., Del Zanna et al. 2004, 2012; Del Zanna 2012a,b;

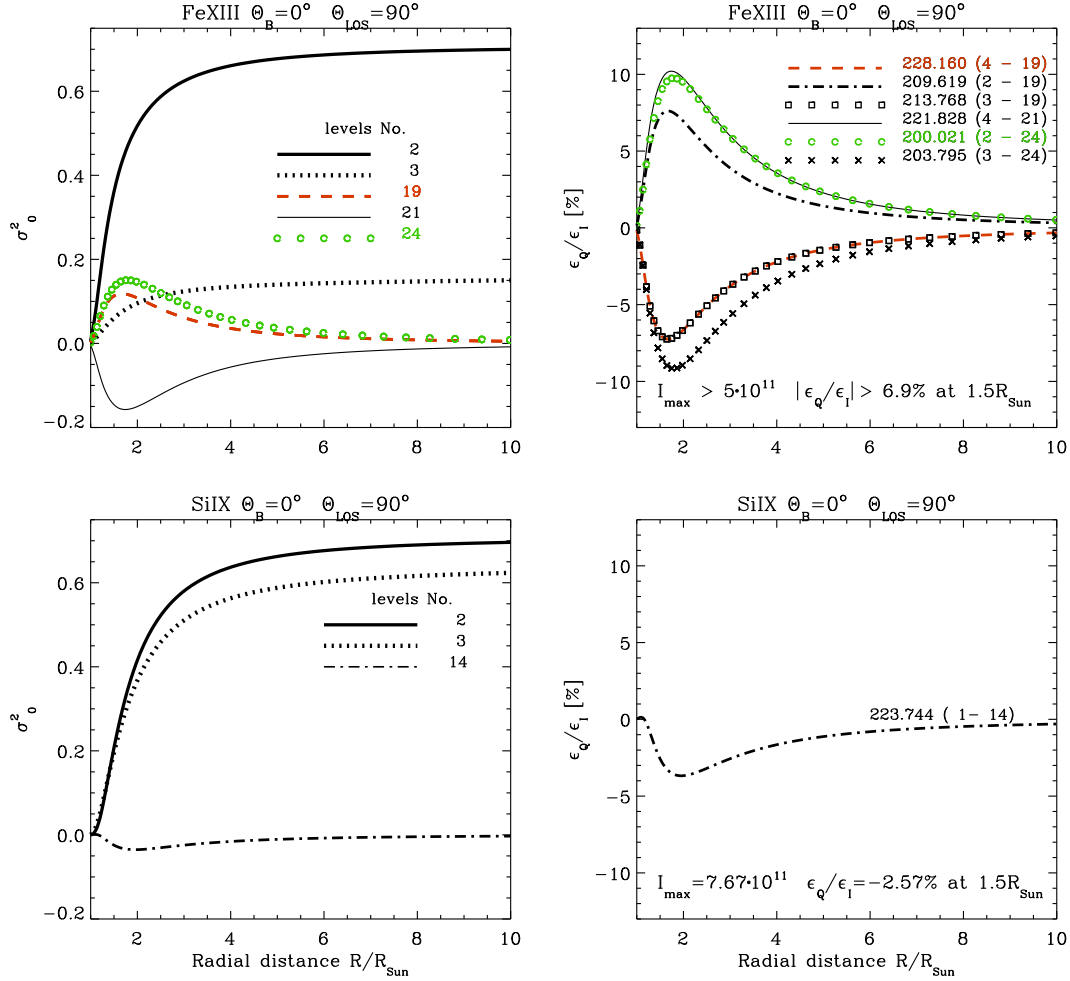


Figure 3. The fractional alignment $\sigma_0^2(\alpha J)$ of the lower and highly excited levels (left panels) and the ratio of the Stokes Q and I emission coefficients $\epsilon_Q(\nu, \Theta)/\epsilon_I(\nu, \Theta)$ (right panels) for selected EUV lines of the Fe XIII and Si IX ions as a function of the radial distance R/R_{Sun} in the coronal model of Del Zanna & DeLuca (2018). The top and bottom panels show the results for the Fe XIII and Si IX ions, respectively. The level numbers, wavelengths, and transitions (in brackets) are indicated in the corresponding panels. Geometrical configuration (Θ_{LOS} is the angle between the solar radius vector through the observed point and the LOS): off-limb observations ($\Theta_{\text{LOS}} = 90^\circ$) of a radial magnetic field ($\Theta_B = 0^\circ$). For all Fe XIII lines shown, the intensity I_{max} at $R/R_{\text{Sun}} = 1.0$ (in units of $10^{11} \text{ photons cm}^{-2} \text{ s}^{-1} \text{ sr}^{-1}$) and the absolute ratio $|\epsilon_Q/\epsilon_I|$ at a radial distance of $R/R_{\text{Sun}} = 1.5$ are equal to or greater than the values indicated at the bottom of the upper-right panel. The intensity I_{max} and the ratio ϵ_Q/ϵ_I at $R/R_{\text{Sun}} = 1.5$ for the Si IX 223.774 Å line are indicated in the bottom section of the lower-right panel. The positive Stokes- Q direction is the perpendicular to the magnetic field.

Del Zanna et al. 2015; Dere et al. 2019; Young et al. 2019; Del Zanna et al. 2021; Dufresne et al. 2024). In our calculations we used the following model atoms given in CHIANTI Version 10 database for the above-mentioned ions (Del Zanna et al. 2021).

Fe X ion—The Fe X model atom has 552 J -levels, 28 556 radiative bound-bound transitions, and 152 076 electron collision bound-bound transitions.

Fe XI ion—The Fe XI model atom is the largest one, with 996 levels, 82 409 radiative bound-bound transitions, and 495 510 electron collision bound-bound transitions.

Fe XIII ion—The Fe XIII model atom has 749 J -levels, 53 418 radiative bound-bound transitions, and 280 126 electron collisional bound-bound transitions.

Fe XIV ion—The Fe XIV model atom has 739 J -levels, 42 667 radiative bound-bound transitions, and 42 666 electron collisional bound-bound transitions. The CHIANTI database for this ion is based mainly on the electron collision calculations by Liang et al. (2010). At the moment, the electron collision matrix for this ion is incomplete, with data only for 1672 transitions.

Si IX ion—The Si IX model atom contains 590 levels, 29 542 radiative bound-bound transitions and 173 755 electron collision bound-bound transitions.

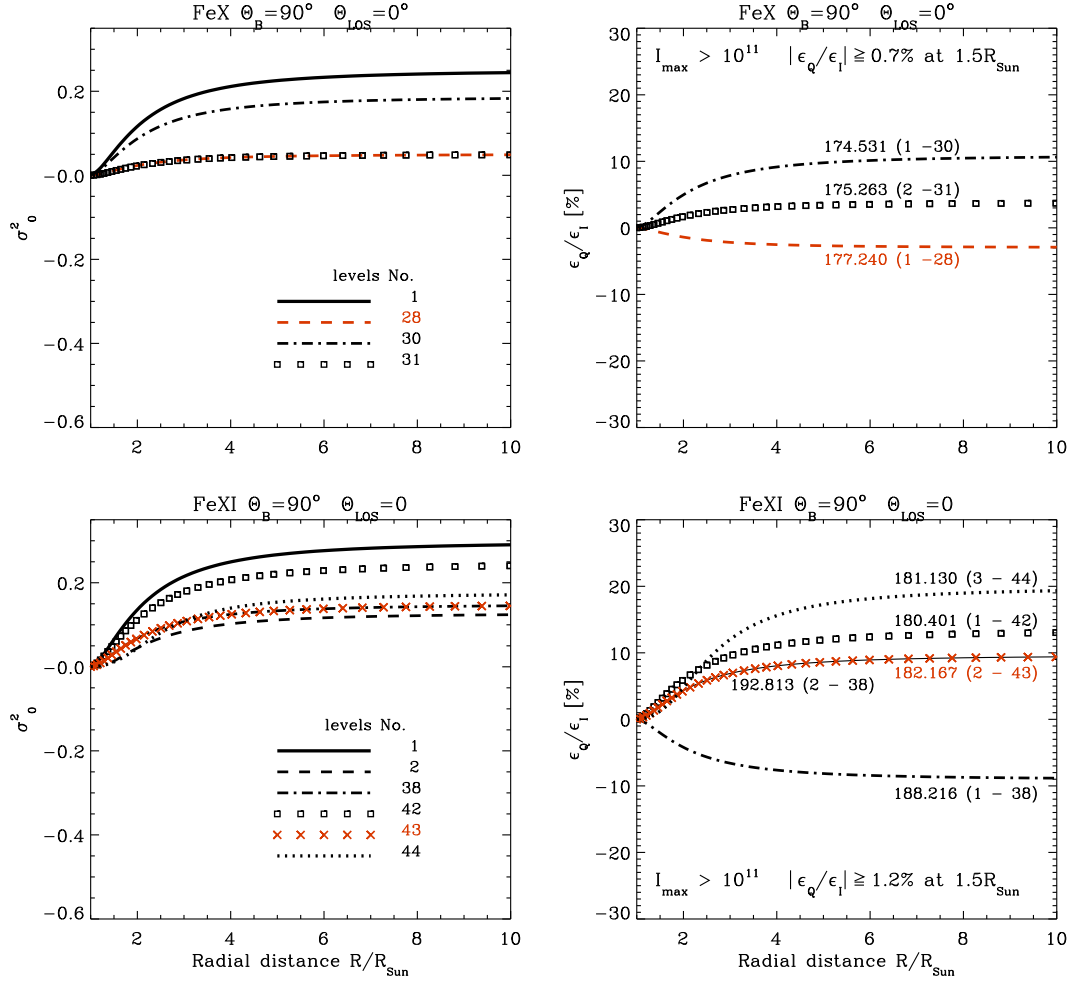


Figure 4. Same as Figure 2, but for the case of observations of a horizontal magnetic field ($\theta_B = 90^\circ$) at the disk center ($\theta_{LOS} = 0^\circ$).

Si x ion—The Si x model atom has 204 J -levels, 5 017 radiative bound-bound transitions and 20 706 electron collision bound-bound transitions.

The comprehensive CHIANTI model atoms described above were considered as reference models to determine less detailed ones with fewer levels and radiative and collisional transitions. We concluded that simplified Fe x, Fe xi, Fe xiii, Fe xiv, Si ix, and Si x model atoms with the first 31, 53, 51, 51, 46, and 25 J -levels, respectively, would be suitable for our investigation. Using such models, the solution of the statistical equilibrium Equations (11) and (12) gives $\rho_0^K(\alpha J)$ values with relative errors smaller than 20%, which imply errors smaller than 5% in the fractional alignment σ_0^2 and in the ratio of emission coefficients ϵ_Q/ϵ_I for the EUV lines considered in this paper. This finding agrees with the results obtained by Del Zanna & Supriya (2025) for the Fe xiii ion.

3.4. IDL code

We have developed an Interactive Data Language (IDL) code for calculating the intensity and polarization of coro-

nal lines based on the formulation of the problem summarized in Section 2. To facilitate the construction of the atomic model needed for the calculations, we have developed also an IDL program in order to obtain any desired simplified model atom starting from the comprehensive model atoms given in the CHIANTI database (Del Zanna et al. 2015; Del Zanna & Mason 2018).

4. RESULTS

We have carried out calculations for each of the coronal ions mentioned above (i.e., Fe x, Fe xi, Fe xiii, Fe xiv, Si ix, and Si x) using the previously indicated model atoms. The calculations have been performed for all heights in the coronal model of Del Zanna & DeLuca (2018) shown in Figure 1, between one and ten solar radii. The larger the height, the larger the anisotropy of the continuum radiation coming from the underlying solar disk, but the smaller the kinetic temperature (which varies between 1.38×10^6 K and 5×10^5 K) and the electron density (which varies between 10^9 and 10^3 cm $^{-3}$). For the physical conditions corresponding to each height in the coronal model we solved the statisti-

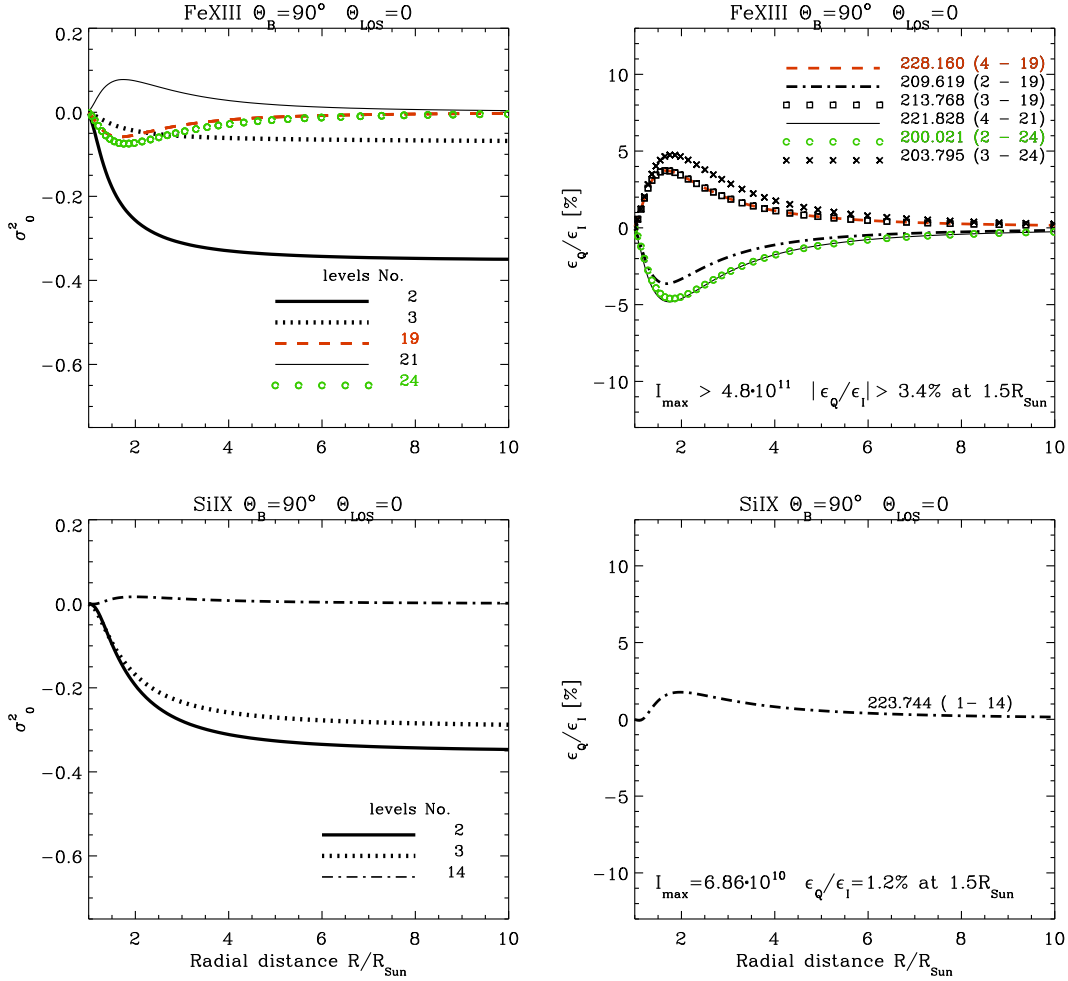


Figure 5. Same as Figure 3, but for the case of observations of a horizontal magnetic field ($\theta_B = 90^\circ$) at the disk center ($\Theta_{LOS} = 0^\circ$).

cal equilibrium equations obtaining the $\rho_0^0(\alpha J)$ and $\rho_0^2(\alpha J)$ multipolar components of the atomic density matrix associated to each J -level in the atomic model under consideration. Then, applying Equations (10), (6), and (7) we calculated the fractional alignment $\sigma_0^2(\alpha J)$ and the Stokes emission coefficients ϵ_I and ϵ_Q for any desired magnetic field inclination and LOS.

Figures 2 – 5 show the results (i.e., σ_0^2 and ϵ_Q/ϵ_I) corresponding to the strongest lines of the following coronal ions:² Fe X, Fe XI, Fe XIII and Si IX. The left panels give $\sigma_0^2(\alpha J)$ for some of the J -levels of the corresponding atomic model and the right panels $\epsilon_Q(\nu, \Theta)/\epsilon_I(\nu, \Theta)$ for some of the per-

mitted EUV lines of the coronal ion under consideration, as a function of height in the used coronal model (up to 10 solar radii). These results are given for two different geometrical and magnetic field configurations: in Figures 2 – 3 for off-limb observations ($\Theta_{LOS} = 90^\circ$) of a radial magnetic field ($\theta_B = 0^\circ$), and in Figures 4 – 5 for disk-center observations ($\Theta_{LOS} = 0^\circ$) of a horizontal magnetic field ($\theta_B = 90^\circ$).

Table 1 gives the list of the infrared and visible forbidden lines that result from transitions between the J -levels of the ground term in the considered coronal ions. Our results indicate that the scattering of the anisotropic continuum radiation of the solar disk that reaches the corona at such forbidden-line wavelengths generates atomic polarization in the ground-term J_ℓ -levels (see the left panels of Figures 2 – 5). More importantly, the upper levels of many permitted EUV lines with Hanle critical magnetic fields $B_H > 2000$ G are also significantly polarized, as a result of the mechanism pointed out by Manso Sainz & Trujillo Bueno (2009): the radiatively-induced atomic alignment of the ground-term levels is partly transferred to the upper levels of the permitted EUV lines via isotropic collisions with electrons. Via sponta-

² We do not show results for the (weaker) permitted EUV lines of Fe IX and Si X because they are similar to those of Fe XIII and Si IX.

Table 1. Forbidden lines of the indicated coronal ions.

Ion	λ (Å)	ℓ	u	$2S+1L_J^{o/e}$		E_ℓ (eV)	E_u (eV)	$A_{u\ell}$ s^{-1}
				low	up			
Fe X	6376.2	1	2	$2P_{3/2}^o$	$2P_{1/2}^o$	0.0	1.94	69.40
Fe XI	7894.0	1	2	$3P_2^e$	$3P_1^e$	0.0	1.57	43.90
Fe XI	61043.0	2	3	$3P_1^e$	$3P_0^e$	1.57	1.77	0.22
Fe XIII	10747.0	1	2	$3P_0^e$	$3P_1^e$	0.0	1.15	14.10
Fe XIII	10798.0	2	3	$3P_1^e$	$3P_2^e$	1.15	2.30	9.88
Fe XIV	5304.4	1	2	$2P_{1/2}^o$	$2P_{3/2}^o$	0.0	2.33	55.20
Si IX	39277.3	1	2	$3P_0^e$	$3P_1^e$	0.0	0.31	0.29
Si IX	25846.5	2	3	$3P_1^e$	$3P_2^e$	0.31	0.79	0.77
Si X	14305.0	1	2	$2P_{1/2}^o$	$2P_{3/2}^o$	0.0	0.86	3.08

NOTE—The columns give the line wavelengths λ , the numbers listing the lower (ℓ) and upper (u) levels of the magnetic dipole line transitions, their $2S+1, L, J$, and parity (o or e) quantum numbers, the level energies E_ℓ , E_u , and the Einstein's coefficients $A_{u\ell}$ for spontaneous emission.

neous emissions this upper-level atomic alignment produces linear polarization in the emitted EUV line radiation. The right panels of the figures give a rough estimation of the fractional linear polarization wavelength-integrated signals as a function of height above the Sun's visible surface.³

In order to qualitatively understand the results shown in Figures 2–5, it is convenient to distinguish between the following two types of coronal ions: those for which the lowest J -level of the ground term can carry atomic alignment (e.g., Fe X with $J_1 = 3/2$ and Fe XI with $J_1 = 2$), and those for which the lowest J -level cannot carry atomic alignment (e.g., Fe XIII and Si IX with $J_1 = 0$, and Fe XIV and Si X with $J_1 = 1/2$). As seen in the right panels of these figures, the variation with the radial distance of the fractional linear polarization signals is different for the EUV lines of such two types of ions. The qualitative explanation of this different behavior is the following, while a more quantitative one can be found in appendices A and B. At any given height in the coronal model of Figure 1 the most populated level is the lowest-energy level of the ion's ground term (i.e., J_1), while the first excited level of the ion's ground term (i.e., level J_2) is significantly less populated, and level J_3 is even less populated. While $N(\alpha_l J_1)/N(\text{ion})$ turns out to be approximately constant with height in the solar coronal model, $N(\alpha_l J_2)/N(\text{ion})$ decreases with height. The J_1 level of the ground term in the Fe X and Fe XI ions can carry

atomic alignment (because J_1 is neither zero nor $1/2$), while in the Fe XIII and Si IX ions (and also in Fe XIV and Si X) the lowest-energy level of the ground-term that can carry atomic alignment is J_2 (see Table 1). The wavelengths of the forbidden-line transitions between the J_1 and J_2 levels of the ion's ground term are 6376.2 Å in Fe X, 7894 Å in Fe XI, 10747 Å in Fe XIII, 5304.4 Å in Fe XIV, 39277.3 Å in Si IX, and 14305 Å in Si X (see Table 1). At these visible and IR wavelengths the continuum radiation coming from the solar disk is significant, and the larger the height in the solar corona the larger the anisotropy of such radiation and the larger the fractional atomic alignment of the J_1 and/or J_2 levels. As explained in Section 1, the alignment of the upper levels of the ion's EUV lines results from the transfer of the atomic alignment in the J -levels of the ground term via inelastic isotropic collisions with electrons. Such a transfer is clearly greater the larger the population of the ground-term J -level that carries atomic alignment because of the scattering of anisotropic radiation in the forbidden line. With these considerations, it is easy to understand the different behavior seen in Figures 2–5 for the two types of coronal ions mentioned above.

5. SELECTION OF THE MOST USEFUL LINES

To provide an initial estimate of the fractional linear polarization Q/I in *off-limb* observations (extending up to 2 solar radii) the Stokes emission coefficients $\varepsilon_Q(\nu, \Theta)$ and $\varepsilon_I(\nu, \Theta)$ were integrated over a path length of ± 10 solar radii along the LOS assuming the physical conditions given by the aforementioned 1D model of the quiet Sun corona. Our estimation indicates that, for the case of off-limb observations, the fractional linear polarization $Q/I \approx \varepsilon_Q/\varepsilon_I$ below $R/R_{\text{Sun}} = 1.5$.

From the extensive list of permitted EUV lines of the Fe X, Fe XI, Fe XIII, Fe XIV, Si IX, and Si X ions with non-zero fractional linear polarization Q/I , we selected the strongest ones. In particular, we considered the off-limb case and focused on EUV permitted lines with wavelength-integrated intensity $I \geq 5 \times 10^{11}$ photons $\text{cm}^{-2} \text{s}^{-1} \text{sr}^{-1}$ at a radial distance $R/R_{\text{Sun}} = 1$ and absolute linear polarization signal $|Q/I| \geq 1\%$ at a radial distance $R/R_{\text{Sun}} = 1.5$. In the 1D coronal model under consideration the intensity at the solar limb can be regarded as an upper limit for off-limb observations. For this reason, we denote this intensity by I_{max} .

In Table 2 we present the list of EUV lines selected according to the two criteria mentioned above, including their atomic parameters, the values of their upper-level Hanle critical magnetic field strength, B_H , their maximum off-limb intensities, I_{max} , as well as their intensity values, I , and the ratio of the Stokes emission coefficients, $\varepsilon_Q(\nu, \Theta)/\varepsilon_I(\nu, \Theta)$, at a radial distance of $R/R_{\text{Sun}} = 1.5$.

The last column of Table 2 indicates that, according to Behring et al. (1976), Del Zanna (2010), and our own iden-

³ This estimation ignores the line of sight integration, because it is just the $\varepsilon_Q/\varepsilon_I$ value in the plane of the sky.

Table 2. EUV lines sensitive to the magnetic field orientation.

λ	ℓ	u	$2S+1L_J^{o/e}$	E_ℓ	E_u	$A_{u\ell}$	B_H	I_{\max}	I	$\varepsilon_Q/\varepsilon_I$	Blends
			low up	(eV)	(eV)		(G)	$1.0R_{\text{Sun}}$	$1.5R_{\text{Sun}}$	$1.5R_{\text{Sun}}$	
Fe X											
177.240	1	28	$^2P_{3/2}^o$	$^2P_{3/2}^e$	0.0	69.95	154.0	13409.5	125.984	0.185	1.368 S (Fe XI 177.232)
174.531	1	30	$^2P_{3/2}^o$	$^2D_{5/2}^e$	0.0	71.04	186.0	17623.5	220.297	0.328	−4.692
175.263	2	31	$^2P_{1/2}^o$	$^2D_{3/2}^e$	1.94	72.69	175.0	25807.0	13.380	0.010	−1.560 B, S (Fe XI 175.270)
Fe XI											
192.813	2	38	$^3P_1^e$	$^3P_2^o$	1.57	65.87	20.7	9016.4	40.081	0.059	−3.910 B, Z, S (Fe XI 192.817)
188.216	1	38	$^3P_2^e$	$^3P_2^o$	0.00	65.87	96.7	9016.4	187.111	0.270	4.015 Z
180.401	1	42	$^3P_2^e$	$^3D_3^o$	0.00	68.73	138.0	11773.9	372.772	0.560	−5.344 Z, S (Fe X 180.441)
182.167	2	43	$^3P_1^e$	$^3D_2^o$	1.57	69.63	104.0	13132.3	54.593	0.065	−3.836
178.058	1	43	$^3P_2^e$	$^3D_2^o$	0.00	69.63	28.5	13132.3	14.953	0.017	3.936 B
180.594	2	44	$^3P_1^e$	$^3D_1^o$	1.57	70.22	55.7	31186.8	12.388	0.007	1.189
181.130	3	44	$^3P_0^e$	$^3D_1^o$	1.77	70.22	78.6	31186.8	17.484	0.010	−2.351 Z
184.793	4	45	$^1D_2^e$	$^1D_2^o$	4.68	71.77	105.0	12541.4	5.024	0.003	−1.572 Z, S (Fe X 184.828)
192.021	2	39	$^3P_1^e$	$^3S_1^o$	1.57	66.14	29.3	6005.6	6.077	0.006	3.271 Z
189.123	2	41	$^3P_1^e$	$^3P_1^o$	1.57	67.13	37.3	9327.9	7.039	0.005	2.515 B, Z
189.711	3	41	$^3P_0^e$	$^3P_1^o$	1.77	67.13	31.0	9327.9	5.852	0.004	−4.907 Z
Fe XIII											
228.160	4	19	$^1D_2^e$	$^3P_2^o$	5.96	60.30	15.80	3941.6	5.454	0.002	−6.925
209.619	2	19	$^3P_1^e$	$^3P_2^o$	1.15	60.30	18.10	3941.6	6.235	0.002	7.260 S (Fe XI 209.622)
213.768	3	19	$^3P_2^e$	$^3P_2^o$	2.30	60.30	18.10	3941.6	6.248	0.002	−6.925 B
221.828	4	21	$^1D_2^e$	$^1D_2^o$	5.96	61.85	38.10	6527.4	7.818	0.002	9.442 S (Fe X 221.813)
200.021	2	24	$^3P_1^e$	$^3D_2^o$	1.15	63.14	25.60	6389.3	8.840	0.002	8.675 B
203.795	3	24	$^3P_2^e$	$^3D_2^o$	2.30	63.14	34.20	6389.3	11.834	0.003	−8.201 S (Fe XIII 203.826)
Si IX											
223.744	1	14	$^3P_0^e$	$^3S_1^o$	0.00	55.41	4.620	2390.0	7.675	0.010	−2.571 S (Fe XIII 223.778)

NOTE—The columns give the line wavelengths λ (in Å), the numbers listing the lower (ℓ) and upper (u) levels of the line transitions, their $2S+1, L, J$, and parity (o or e) quantum numbers, the level energies E_ℓ, E_u , the Einstein's coefficients for spontaneous emission, $A_{u\ell}$ (in units of 10^9 s^{-1}), the critical field strength B_H , the intensities I_{\max} at $R/R_{\text{Sun}} = 1.0$, the intensities I at $R/R_{\text{Sun}} = 1.5$ (integrated over a path length of ± 10 solar radii along the LOS), given in units of $10^{11} \text{ photons cm}^{-2} \text{ s}^{-1} \text{ sr}^{-1}$, and the ratio of the Stokes emissivity coefficients $\varepsilon_Q(\nu, \Theta)/\varepsilon_I(\nu, \Theta) \approx Q/I$ (in %) at $R/R_{\text{Sun}} = 1.5$ outside the limb calculated for radial magnetic field ($\theta_B = 0^\circ$). The last column provides information about blends with other lines.

References—The letter B indicates Behring et al. (1976), Z refers to Del Zanna (2010, 2012a), and S to this study. The symbols in brackets indicate the ion and wavelength of the spectral line blends when assuming that the spectral resolution is worse than 0.05 Å .

tification, some of these EUV lines are blended. Therefore, their possible usefulness for coronal magnetometry needs to be clarified.

We emphasize that the intensity I_{\max} and the ratio $\varepsilon_Q/\varepsilon_I$ presented in Table 2 are given only for off-limb observations ($\Theta_{\text{LOS}} = 90^\circ$) of a radial magnetic field ($\theta_B = 0^\circ$). Our calculations indicate that, for observations of a horizontal field ($\theta_B = 90^\circ$) at the solar disk center ($\Theta_{\text{LOS}} = 0^\circ$), the absolute values of this ratio for the selected EUV lines are approximately half as large.

Finally, we point out that, in addition to the EUV lines listed in Table 2, there are other EUV lines of the Fe X, Fe XI, Fe XIII, Fe XIV, Si IX, and Si X ions that have relatively low values of the Hanle critical magnetic field strength B_H (see Table 3). In principle, the linear polarization of these coronal lines can be sensitive to the coronal magnetic field strength, because they are not in the saturated regime of the Hanle effect. However, for the Hanle effect to operate in these EUV permitted lines, upper-level coherences in the magnetic field reference frame must be present. Under the assumption of isotropic collisions this would be only possible if there is

Table 3. EUV lines sensitive to the strength and orientation of the magnetic field.

λ	ℓ	u	$^{2S+1}L_J^{o/e}$		E_ℓ	E_u	$A_{u\ell}$	B_H	$0.2B_H - 5B_H$		I_{\max}	Blends
(Å)			low	up	(eV)	(eV)		(G)	(G)		$1.0R_{\text{Sun}}$	
Fe x												
225.856	1	19	$^2P_{3/2}^o$	$^2D_{5/2}^e$	0.0	54.90	0.152	14.4	2.9	72.0	6.243	B
Fe xi												
369.163	2	6	$^3P_1^e$	$^3P_2^o$	1.57	35.16	0.725	235.9	47.2	1179.5	20.666	
352.670	1	6	$^3P_2^e$	$^3P_2^o$	0.00	35.16	2.320	235.9	47.2	1179.5	66.088	
356.519	2	7	$^3P_1^o$	$^3P_1^o$	1.57	36.35	0.781	249.7	49.9	1248.5	9.002	
358.613	3	7	$^3P_0^o$	$^3P_1^o$	1.77	36.35	0.998	249.7	49.9	1248.5	11.513	
341.113	1	7	$^3P_2^o$	$^3P_1^o$	0.00	36.35	1.500	249.7	49.9	1248.5	17.295	
257.772	1	12	$^3P_2^e$	$^5D_2^o$	0.00	48.10	0.0572	4.4	0.9	22.0	8.601	B, Z
257.554	1	13	$^3P_2^e$	$^5D_3^o$	0.00	48.14	0.0197	1.5	0.3	7.5	16.818	Z, S (Fe xiii 257.510)
242.215	1	15	$^3P_2^e$	$^3D_2^o$	0.00	51.19	0.0358	5.1	1.0	25.5	6.388	Z
240.717	1	16	$^3P_2^e$	$^3D_3^o$	0.00	51.51	0.0018	0.2	0.04	1.0	10.406	B, Z, S (Fe xiii 240.696)
206.258	1	29	$^3P_2^e$	$^3P_1^o$	0.00	60.11	2.410	214.6	42.9	1073.0	5.810	Z, S (Fe xi 206.268)
202.424	1	34	$^3P_2^e$	$^3P_2^o$	0.00	61.25	4.660	445.2	89.0	2226.0	13.711	Z, S (Fe xi 202.450)
201.112	1	35	$^3P_2^e$	$^3D_3^o$	0.00	61.65	0.449	42.7	8.5	213.5	6.169	B, Z, S (Fe xiii 201.126)
Fe xiii												
359.644	2	8	$^3P_1^e$	$^3D_2^o$	1.15	35.63	1.450	147.5	29.5	737.5	13.856	
Fe xiv												
353.83	2	7	$^2P_{3/2}^o$	$^2D_{5/2}^e$	2.34	37.38	1.970	186.7	37.3	933.5	3.773	
Si ix												
345.121	2	7	$^3P_1^e$	$^3D_2^o$	0.32	36.24	2.070	241.3	48.3	1206.5	38.043	
292.759	2	12	$^3P_1^e$	$^3P_2^o$	0.32	42.67	1.390	511.0	102.2	2555.0	10.260	S (Si ix 292.808)
349.792	3	7	$^3P_2^e$	$^3D_2^o$	0.80	36.24	0.405	241.3	48.3	1206.5	7.466	S (Fe xi 349.772)
349.860	3	9	$^3P_2^e$	$^3D_3^o$	0.80	36.23	2.380	203.4	40.7	1017.0	41.112	
296.113	3	12	$^3P_2^e$	$^3P_2^o$	0.80	42.67	5.350	511.0	102.2	2555.0	39.506	B
Si x												
356.037	2	7	$^2P_{3/2}^o$	$^2D_{5/2}^e$	0.87	35.69	2.037	193.0	38.6	965.0	53.629	S (Si x 356.049)

NOTE—Similar to Table 2, but for EUV lines that can in principle be sensitive to the magnetic field strength and orientation. The two columns to the right of B_H indicate the approximate range of magnetic sensitivity to the Hanle effect (i.e., $0.2B_H < B < 5B_H$) of the indicated EUV lines.

a significant impact of anisotropic radiation pumping at the EUV line wavelengths (e.g., [Seaton et al. 2025](#)), which is a possibility that should be carefully investigated in the future.

6. SUMMARY & CONCLUSIONS

The EUV radiation from permitted line transitions in highly ionized ions (e.g., Fe X, Fe XI, Fe XIII, Fe XIV, Si IX, and Si X) is produced by the million-degree plasma of the solar corona. In the solar corona the excitation of the upper levels of such transitions is mainly due to inelastic collisions with electrons. At coronal heights the radiation coming from the underlying solar disk is very anisotropic, but at EUV wavelengths the intensity of this solar-disk radiation is too low so as to produce any significant radiative pumping. How-

ever, as is well known, the radiation coming from the solar disk is very significant at the near-IR and visible wavelengths of the coronal forbidden lines that result from transitions between the J -levels of the ion's ground-term, and the ensuing anisotropic radiation pumping induces atomic alignment in such ground-term levels. [Manso Sainz & Trujillo Bueno \(2009\)](#) pointed out that this radiatively-induced atomic alignment of the ground-term levels can be partly transferred to the upper levels of some EUV permitted lines via isotropic inelastic collisions with electrons, that the ensuing spontaneous emission produces linear polarization in the permitted EUV line under consideration, and that this polarization is sensitive to the orientation of the magnetic field. In addition to confirming their quantitative results for the Fe X lines at

174.5 Å and 177 Å, in this work we have investigated the polarization produced by such mechanism in the permitted EUV lines of Fe X, Fe XI, Fe XIII, Fe XIV, Si IX, and Si X, providing lists of the most interesting lines for further future studies.

Figures 2 – 5 show the results obtained for the Fe X, Fe XI, Fe XIII, and Si IX coronal ions, at each height in the 1D model of Figure 1. As seen in these figures, the variation with the radial distance of $\varepsilon_Q(\nu, \Theta)/\varepsilon_I(\nu, \Theta)$ is different for the permitted EUV lines of Fe X and Fe XI compared with those of Fe XIII and Si IX. As explained in Section 4, this is because the lowest J -level of the ion’s ground term that can carry atomic alignment is J_1 for Fe X and Fe XI, while it is J_2 for Fe XIII and Si IX (J_1 being the lowest J -level and J_2 the first excited J -level of the ion’s ground term). The key point here is that the fractional overall population of the J_1 level (i.e., $N(\alpha_l J_1)/N(\text{ion})$) is approximately constant with height, while $N(\alpha_l J_2)/N(\text{ion})$ decreases with height. Consequently, since the alignment of the upper level of the EUV line under consideration results from the collisional transfer of the alignment present in the line’s lower level, the variation with the radial distance of the resulting upper-level fractional alignment is different for the two types of coronal ions mentioned above.

The permitted EUV lines given in Table 2 are those for which the critical magnetic field for the operation of the Hanle effect in their upper-level is larger than 2000 G, reason why their linear polarization signals are sensitive to the orientation of the magnetic field, but not to its strength. The lines given in Table 3 have much smaller critical Hanle fields and, in principle, they can be sensitive to the orientation and the strength of the coronal magnetic field. However, for the Hanle effect to operate in these EUV lines it would be nec-

essary to have radiatively-induced upper-level coherences in the magnetic field reference frame.

In order to be able to measure the predicted polarization signals, it is crucial to choose the EUV lines with the largest number of emitted solar photons. Of the permitted EUV lines we have investigated, the most intense EUV lines are the Fe X lines at 174.531 Å and 177.240 Å, and the Fe XI lines at 188.216 Å and 180.401 Å. However, from these lines the only one that is not blended is the Fe X line at 174.531 Å.

The next step of our investigation will be to provide predictions from calculations in state-of-the-art three-dimensional models of the million-degree plasma of coronal structures, along with estimations of the exposure times needed for measuring the predicted polarization signals assuming reasonable spatial and temporal resolutions.

7. ACKNOWLEDGMENTS

We are grateful to Tanausú del Pino Alemán (IAC) for suggesting improvements to an earlier version of this paper, as well as to the anonymous referee for carefully studying the paper and providing valuable inputs for enhancing the presentation. We acknowledge financial support from the European Research Council (ERC) under the European Union’s Horizon 2020 research and innovation program (ERC Advanced Grant agreement No 742265). NGS is grateful to the Fundación Occident for funding two working visits at the IAC. JTB and SHD acknowledge support from the Agencia Estatal de Investigación del Ministerio de Ciencia, Innovación y Universidades (MCIU/AEI) under the grant “Polarmetric Inference of Magnetic Fields” and the European Regional Development Fund (ERDF) with reference PID2022-136563NB-I00/10.13039/501100011033.

REFERENCES

- Allen, C. W. 1976, *Astrophysical Quantities*, 3rd edn. (University of London, Athlone Press)
- Asplund, M., Amarsi, A. M., & Grevesse, N. 2021, *A&A*, 653, A141
- Asplund, M., Grevesse, N., Sauval, A. J., & Scott, P. 2009, *ARA&A*, 47, 481
- Behring, W. E., Cohen, L., Feldman, U., & Doschek, G. A. 1976, *ApJ*, 203, 521
- Bhatia, A. K., & Doschek, G. A. 1995, *Atomic Data and Nuclear Data Tables*, 60, 97
- Casini, R., & Judge, P. G. 1999, *ApJ*, 522, 524
- Del Zanna, G. 2010, *A&A*, 514, A41
- . 2012a, *A&A*, 537, A38
- . 2012b, *A&A*, 546, A97
- Del Zanna, G., Berrington, K. A., & Mason, H. E. 2004, *A&A*, 422, 731
- Del Zanna, G., & DeLuca, E. E. 2018, *ApJ*, 852, 52
- Del Zanna, G., Dere, K. P., Young, P. R., & Landi, E. 2021, *ApJ*, 909, 38
- Del Zanna, G., Dere, K. P., Young, P. R., Landi, E., & Mason, H. E. 2015, *A&A*, 582, A56
- Del Zanna, G., & Mason, H. E. 2018, *Living Reviews in Solar Physics*, 15, 5
- Del Zanna, G., Storey, P. J., Badnell, N. R., & Mason, H. E. 2012, *A&A*, 541, A90
- Del Zanna, G., & Supriya, H. D. 2025, *MNRAS*, 537, 3781
- Dere, K. P., Del Zanna, G., Young, P. R., Landi, E., & Sutherland, R. S. 2019, *ApJS*, 241, 22

- Dufresne, R. P., Del Zanna, G., Young, P. R., et al. 2024, *ApJ*, 974, 71
- Gibson, S. E., Fludra, A., Bagenal, F., et al. 1999, *J. Geophys. Res.*, 104, 9691
- Judge, P. G., Low, B. C., & Casini, R. 2006, *ApJ*, 651, 1229
- Khan, R., Gibson, S. E., Casini, R., & Nagaraju, K. 2024, *ApJ*, 971, 27
- Laming, J. M. 2015, *Living Reviews in Solar Physics*, 12, 2
- Landi Degl’Innocenti, E., & Landolfi, M. 2004, *Polarization in Spectral Lines*, Vol. 307 (Kluwer Academic Publishers), doi:10.1007/978-1-4020-2415-3
- Liang, G. Y., Badnell, N. R., Crespo López-Urrutia, J. R., et al. 2010, *ApJS*, 190, 322
- Manso Sainz, R., & Trujillo Bueno, J. 2009, in *Astronomical Society of the Pacific Conference Series*, Vol. 405, *Solar Polarization 5: In Honor of Jan Stenflo*, ed. S. V. Berdyugina, K. N. Nagendra, & R. Ramelli, 423
- Mihalas, D. 1978, *Stellar atmospheres*, 2nd edn. (W.H. Freeman & Co.)
- Raouafi, N. E., Lemaire, P., & Sahal-Bréchet, S. 1999, *A&A*, 345, 999
- Raouafi, N. E., Sahal-Bréchet, S., & Lemaire, P. 2002, *A&A*, 396, 1019
- Schad, T., & Dima, G. 2020, *SoPh*, 295, 98
- . 2021, *SoPh*, 296, 166
- Schmelz, J. T., Reames, D. V., von Steiger, R., & Basu, S. 2012, *ApJ*, 755, 33
- Seaton, D. B., Downs, C., Del Zanna, G., et al. 2025, arXiv e-prints, arXiv:2504.08996
- Shchukina, N., Sukhorukov, A., & Trujillo Bueno, J. 2012, *ApJ*, 755, 176
- Shchukina, N., & Trujillo Bueno, J. 2001, *ApJ*, 550, 970
- Supriya, H. D., de Vicente, A., del Pino Alemán, T., Trujillo Bueno, J., & Shchukina, N. 2025, *ApJ*, in press, (see arXiv:2505.05962)
- Supriya, H. D., Trujillo Bueno, J., de Vicente, A., & del Pino Alemán, T. 2021, *ApJ*, 920, 140
- Testa, P., Martínez-Sykora, J., & De Pontieu, B. 2023, *ApJ*, 944, 117
- Trujillo Bueno, J. 2001, in *Astronomical Society of the Pacific Conference Series*, Vol. 236, *Advanced Solar Polarimetry – Theory, Observation, and Instrumentation*, ed. M. Sigwarth, 161
- Trujillo Bueno, J., & del Pino Alemán, T. 2022, *ARA&A*, 60, 415
- Vásquez, A. M., van Ballegoijen, A. A., & Raymond, J. C. 2003, *ApJ*, 598, 1361
- Withbroe, G. L., & Raymond, J. C. 1984, *ApJ*, 285, 347
- Young, P. R., Dere, K. P., Del Zanna, G., Landi, E., & Sutherland, R. 2019, in *American Astronomical Society Meeting Abstracts*, Vol. 234, *American Astronomical Society Meeting Abstracts #234*, 314.02

APPENDIX

In the following two appendices we discuss in more detail the atomic polarization of the J -levels of the ground term (Appendix A) and of the upper levels of the permitted EUV lines studied in this paper (Appendix B).

A. ATOMIC POLARIZATION OF THE GROUND-TERM LEVELS

As discussed in Section 4, there are two types of coronal ions in Table 2: those for which the lowest J -level of the ground term can carry atomic alignment (e.g., Fe X with $J_1 = 3/2$ and Fe XI with $J_1 = 2$), and those for which the lowest J -level cannot carry atomic alignment (e.g., Fe XIII and Si IX with $J_1 = 0$, Fe XIV and Si IX with $J_1 = 1/2$).

Figures 2 and 4 show results for the first type of ions, while results for the second type are given in Figures 3 and 5. The wavelengths of the forbidden-line transitions between the ground-term J -levels are given in Table 1. At these visible and IR forbidden-line wavelengths the solar-disk continuum radiation is significant, and the larger the height in the solar corona the larger the anisotropy of such radiation and the larger the absolute value of the fractional atomic alignment σ_0^2 of the J_1 levels of the Fe X and Fe XI ions and of the first excited J_2 ground-term levels of the Fe XIII and Si IX ions (see left panels of Figures 2 – 5). Additionally, the J_2 level (i.e., $^3P_1^e$) of the Fe XI ion also carries atomic polarization, due to scattering of the incident anisotropic continuum radiation in the forbidden 61043 Å line, but its σ_0^2 absolute value, which increases with height, remains smaller. Likewise, the third excited J_3 levels of the Fe XIII and Si IX ground terms are also polarized by anisotropic radiation pumping in the forbidden-line transitions at the 10798 Å and 25846.5 Å infrared wavelengths, which occur between the J_2 and J_3 levels (see Table 1). The fractional alignment σ_0^2 of these J_3 levels also increases with height, but remains lower than that of the J_2 levels. Such a different behavior of the σ_0^2 values for the J_1 , J_2 and J_3 levels of the ground term is easy to understand if one takes into account that the overall population of the J_1 level is larger than that of level J_2 , and this larger than that of level J_3 .

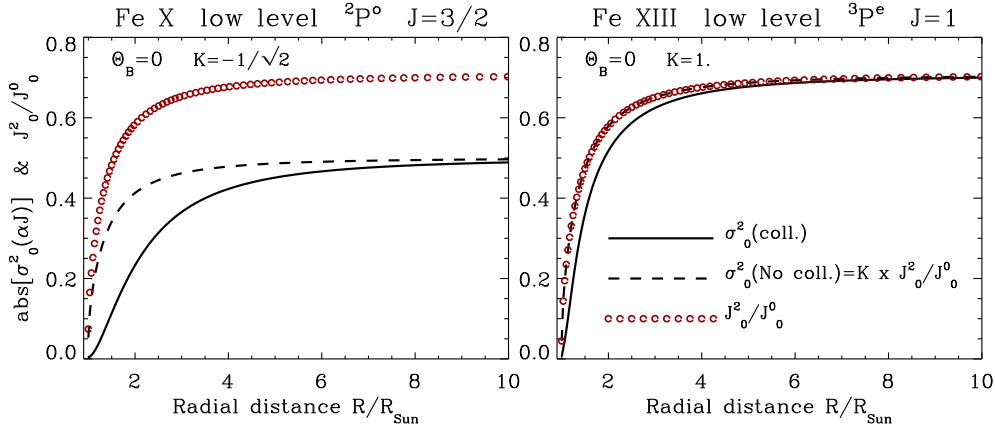


Figure 6. Fractional alignment $\sigma_0^2(\alpha_\ell J_\ell)$ of the first $^2P_{3/2}^0$ J_1 -level of the Fe X ground term (left panel) and of the second $^3P_1^e$ J_2 -level of the Fe XIII ground term (right panel) as a function of the radial distance R/R_{Sun} in the spherically symmetric 1D quiet-Sun coronal model of Figure 1. Solid lines: $\sigma_0^2(\alpha_\ell J_\ell)$ values calculated taking into account electron collisions. Dashed lines: $\sigma_0^2(\alpha_\ell J_\ell)$ values obtained in the absence of collisions. Red circles: anisotropy of the continuum radiation at 6376 Å (for Fe X) and at 10747 Å (for Fe XIII). The results shown are for the case of a vertical magnetic field ($\theta_B = 0^\circ$).

The results presented in Figure 6 facilitate a more detailed understanding of the atomic polarization behavior of the ground-term levels of the Fe X, Fe XI, Fe XIII, Fe XIV, Si IX, and Si X ions. This figure shows results only for the Fe X and Fe XIII ions, because the results for other ions are similar. Figure 6 shows that in the absence of electron collisions the fractional alignment $\sigma_0^2(\alpha_\ell J_\ell)$ of the lower levels of the ground term is proportional to the anisotropy of the incident continuum radiation

$$\sigma_0^2(\alpha_\ell J_\ell) = K \times \frac{J_0^2}{J_0^0} \quad (\text{A1})$$

at 6376 Å (for Fe X) and at 10747 Å (for Fe XIII).

The value of the coefficient K depends on which of the levels of the ground term turns out to be polarized. For the Fe X and Fe XI ions, whose lowest level of the ground term that is aligned is J_1 , $K = -1/\sqrt{2}$. For the Fe XIII, Fe XIV, Si IX, and Si X ions, the lowest level of the ground term that is aligned is J_2 . In this case, $K = 1$ for Fe XIII, Si IX, and Si X, while $K = +1/\sqrt{2}$ for Fe XIV and Si IX.

Our calculations show that if inelastic collisions with electrons are accounted for, the fractional alignment $\sigma_0^2(\alpha_\ell J_\ell)$ is very well described by formula (6) of Manso Sainz & Trujillo Bueno (2009). The only change is that in the general case this formula contains a coefficient K that coincides with $-1/\sqrt{2}$ only for the Fe X and Fe XI ions. Finally, it should be emphasized that for the case of an inclined magnetic field the coefficient K has to be multiplied by the factor $(3\cos^2\theta_B - 1)$. As a result, for the case of a horizontal magnetic field ($\theta_B = 90^\circ$) observed at the solar disk center ($\Theta_{\text{LOS}} = 0^\circ$), the absolute values of $\sigma_0^2(\alpha_\ell J_\ell)$ are actually a factor two lower than for the case of a radial magnetic field ($\theta_B = 0^\circ$) observed off-limb in 90° scattering geometry ($\Theta_{\text{LOS}} = 90^\circ$). A careful comparison of the $\sigma_0^2(\alpha_\ell J_\ell)$ values corresponding to these two cases (compare Figures 2 and 3 with Figures 4 and 5), confirms this conclusion.

Figure 6 shows that in the 1D coronal model under consideration the inelastic collisions with electrons reduce the atomic polarization of the ground-term lower levels. The electron number density decreases with height and, as a result, the lower-level fractional polarization $\sigma_0^2(\alpha_\ell J_\ell)$ tends to the maximum value corresponding to Equation (A1).

B. ATOMIC POLARIZATION OF THE UPPER LEVELS OF THE EUV LINES

A comparison of Figures 2 and 3 with Figures 4 and 5 reveals that for the EUV lines with $B_H > 2000$ G, the fractional alignment $\sigma_0^2(\alpha_u J_u)$ of their upper levels and the ratio of their Stokes emissivity coefficients $\varepsilon_Q/\varepsilon_I$ show two types of variations with the radial distance R/R_{Sun} .

As shown in Figures 2 and 4 the variation with the radial distance of the absolute values of $\sigma_0^2(\alpha_u J_u)$ and $\varepsilon_Q/\varepsilon_I$ for the Fe X and Fe XI EUV lines initially increases rapidly, then the rate of increase slows down and, finally, starting at $R/R_{\text{Sun}} \approx 6$, the $\sigma_0^2(\alpha_u J_u)$ and $\varepsilon_Q/\varepsilon_I$ values remain constant.

In contrast to the aforementioned EUV lines, the height dependence of such quantities for the Fe XIII and Si IX EUV lines is different (see Figures 3 and 5). Initially, the absolute values of $\sigma_0^2(\alpha_u J_u)$ and $\varepsilon_Q/\varepsilon_I$ also increase with height; however, at distances around $R/R_{\text{Sun}} \approx 1.5 - 3$, these quantities reach a maximum value before subsequently decreasing. A similar behavior is found for the EUV lines of the Fe XIV and Si X ions.

In order to explain this different behavior of the EUV lines in such two groups of coronal ions, we approximated the fractional alignment $\sigma_0^2(\alpha_u J_u)$ of their upper levels using the following expression:

$$\sigma_0^2(\alpha_u J_u) = \sigma_0^2(\alpha_\ell J_\ell) \times F(N_e, T_e) \quad (\text{B2})$$

where $\sigma_0^2(\alpha_\ell J_\ell)$ is the fractional alignment of the lower level of the line under consideration, and $F(N_e, T_e)$ is a function that depends on the coronal electron density N_e and the kinetic temperature T_e . This expression provides a very good approximation to the results obtained with Equation (10) for $\sigma_0^2(\alpha_u J_u)$ when using the ρ_0^2 and ρ_0^0 values that result from the solution of the statistical equilibrium Equations (11) and (12). The linear Pearson correlation coefficient between the approximate and exact $\sigma_0^2(\alpha_u J_u)$ values exceeds 0.99.

The function $F(N_e, T_e)$ primarily depends on the density matrix element

$$\rho_0^0(\alpha_\ell J_\ell) = \frac{N(\alpha_\ell J_\ell)}{N(\text{ion})} \times \frac{1}{\sqrt{(2J_\ell + 1)}}, \quad (\text{B3})$$

which in turn is proportional to the relative population $N(\alpha_\ell J_\ell)/N(\text{ion})$ of the lower J_ℓ level. For the case of the Fe X and Fe XI ions the lower level J_ℓ is J_1 (i.e., the lowest-energy level of the ground term). For the Fe XIII, Fe XIV, Si IX, and Si X ions, it is J_2 (i.e., the first excited level of the ground term).

Considering that in the solar corona the vast majority of ions are in the J_1 level, it is expected that the ratio $N(\alpha_\ell J_1)/N(\text{ion})$ and, hence, the function $F(N_e, T_e)$ will vary only slightly with the radial distance R/R_{Sun} . On the other hand, the ratio $N(\alpha_\ell J_2)/N(\text{ion})$ decreases rapidly with increasing radial distance. Consequently, the function $F(N_e, T_e)$ must also decrease with height.

Figure 7 illustrates the dependence of $\rho_0^0(\alpha_\ell J_\ell)$, $\sigma_0^2(\alpha_\ell J_\ell)$, $\sigma_0^2(\alpha_u J_u)$, and $F(N_e, T_e)$ on the radial distance R/R_{Sun} , for the Fe X 174.531 Å and Fe XIII 202.021 Å lines. Results for the Fe X and Fe XIII lines are shown in the left and right panels, respectively. The top panels of this figure show that the height dependence of the density-matrix element $\rho_0^0(\alpha_\ell J_\ell)$ for the Fe X ground-term level J_1 and for the Fe XIII ground-term level J_2 is very different. As we can see, the values of $\rho_0^0(\alpha_\ell J_1)$ for the

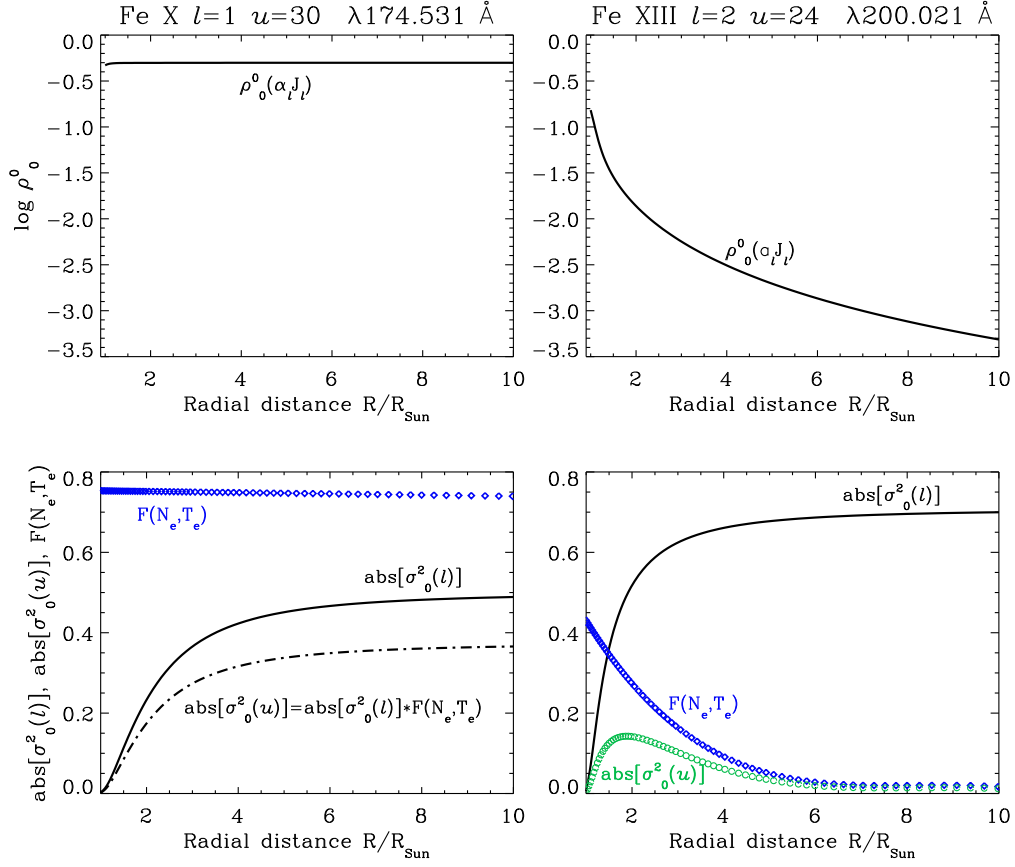


Figure 7. The left and right panels show results for the Fe X and Fe XIII lines, respectively. Top panels: the density matrix elements $\rho_0^0(\alpha_\ell J_\ell)$. Bottom panels: the term $F(N_e, T_e)$, the fractional alignment $\sigma_0^2(\alpha_\ell J_\ell)$ (lower level) and the fractional alignment $\sigma_0^2(\alpha_u J_u)$ (upper level) for the Fe X 174.531 Å and Fe XIII 202.021 Å lines as a function of the radial distance R/R_{Sun} in the spherically symmetric 1D quiet-Sun coronal model of Figure 1.

lower level of the Fe X 174.531 Å line changes very little with height, while the values of $\rho_0^0(\alpha_\ell J_\ell)$ for the lower level of the Fe XIII 202.021 Å line decreases by nearly three orders of magnitude.

The bottom panels of Figure 7 show the variation with the radial distance of the function $F(N_e, T_e)$ for both types of ions. Its behavior (see the blue curve) is similar to that of $\rho_0^0(\alpha_\ell J_\ell)$. For the Fe X ion, F remains nearly constant throughout the corona, whereas for the Fe XIII ion F decreases rapidly with increasing radial distance. As a result, the shape of the variation with the radial distance of the absolute value of $\sigma_0^2(J_u)$ for the highly excited upper level J_{30} of the Fe X 174.531 Å line is similar to that of $\sigma_0^2(J_\ell)$. This is because according to Equation B2, the variation with the radial distance of $\sigma_0^2(J_u)$ follows that of the product of the (nearly constant) function F and the (increasing with height) absolute value of the fractional alignment $\sigma_0^2(J_\ell) = \sigma_0^2(J_1)$.

The bottom right panel of Figure 7 shows that for the Fe XIII 202.021 Å line the shape of the variation with the radial distance of the absolute value of $\sigma_0^2(J_u)$ is that given by the green-circles curve, which follows that of the product of the (decreasing with height) function F and the (increasing with height) absolute value of the fractional alignment $\sigma_0^2(J_\ell) = \sigma_0^2(J_2)$.

Finally, we point out that the above-mentioned results for the EUV lines of Fe X are similar to those of Fe XI. Likewise, the results obtained for the EUV lines of Fe XIII are similar to those of the Fe XIV, Si IX, and Si X ions.